CDF/DOC/BOTTOM/PUBLIC/6361 v2
December 14, 2004

COT dE/dx Measurement and Corrections

Shin-Shan Yu, Joel Heinrich, Nigel Lockyer
Dave Ambrose, Peter Wittich
University of Pennsylvania

Abstract

This document first describes how dE/dx in the COT is measured. Then it describes the correction applied on the raw dE/dx. The correction code is available from CDF software newer than 4.8.3. These corrections remove the dE/dx dependence on the dip angle θ, aspect angle, drift distance, superlayer, wire, high voltage and pressure in the COT. Finally the dE/dx resolution is presented and we show that the system performance achieved meets the goals of the CDF Run II Technical Design Report [9].

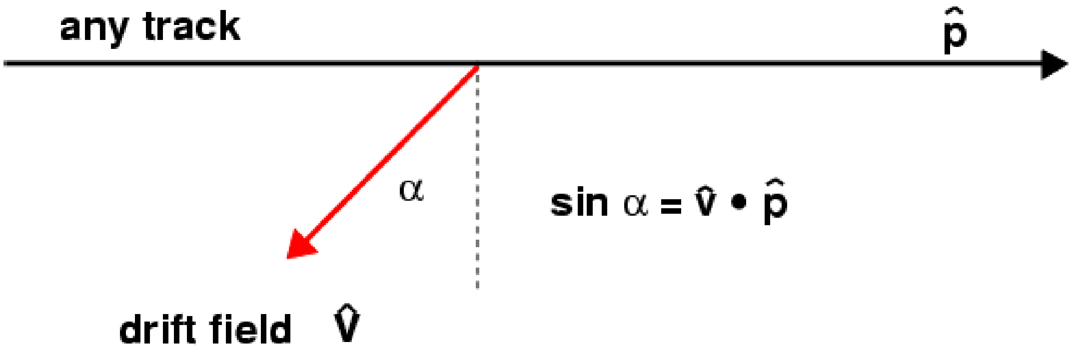

Figure 1: Aspect angle definition. The red solid line is the drift field. The black solid line represents any random track. The dashed line is the normal of the track. $\hat{v}$ is the unit vector along the drift field direction, $\hat{p}$ is the unit vector along the track momentum direction.

1 dE/dx Terminology

COT	Central Outer Tracker, the drift chamber at CDF.
ASDQ	COT front-end electronics, including the amplifier, shaper, discriminator and Q (charge) measurement.
TDC	Time to Digital Converter.
Universal Curve	A curve or formula obtained by fitting dE/dx as a function of $\beta\gamma$, which predicts dE/dx of all stable charged particles, and is therefore universal.
QDR	Charge drain current setting in the ASDQ, controlling the ASDQ digital pulse width as a function of the charge.
TREFE/TREFO	Calibration voltage settings in the ASDQ for even and odd channels, which determine the amount of charge injected by the calibration circuit.
Aspect Angle	The angle of the track with respect to the drift field direction minus 90 degrees, denoted as α (see Figure 1).
Drift Distance	The distance between the wire and the mid-point of a track segment in the drift field direction.
Cell Tilt Angle	35 degrees, to accommodate the magnetic field and make a radial track perpendicular to the drift field as much as possible.

2 dE/dx Measurement at the COT

2.1 Physics Background

dE/dx is defined as the energy loss per unit length in the media. In this note, we are concerned with the energy loss through ionization, which is particularly useful for particle identification. When a charged particle traverses the gas volume of the drift chamber, it leaves a trail of ionization along its flight path. Its energy loss in the chamber is proportional to the amount of ionization, or the amount of charge deposited. The average total energy loss per unit length can be described by the Bethe-Bloch formula [1].

$$\frac{dE}{dx} = \frac{4\pi N e^4}{mc^2\beta^2} z^2 \left(\ln \frac{2mc^2\beta^2\gamma^2}{I} - \beta^2 - \frac{\delta(\beta)}{2}\right) \tag{1}$$

$N \equiv$ number density of electrons in the medium
$m \equiv$ electron mass
$z \equiv$ incident particle charge
$I \equiv$ mean excitation energy of the medium atoms
$\beta = v/c$
$\gamma = 1/(1-\beta^2)$
$\delta(\beta) =$ correction of the density effect at high β

Equation 1 shows that for a drift chamber with fixed gas properties, dE/dx only depends on the particle velocity $\beta\gamma$. Combined with a measurement of the momentum, dE/dx can be used to distinguish particles of different mass. As shown in Figure 2 [2], stable particles in the detector like e, μ, π, K and protons have quite different dE/dx in certain momentum regions. The difference between two particle types divided by the dE/dx resolution is the separation power. The separation power is a function of momentum.

However, the COT is not optimized for dE/dx measurement. It is mainly designed for tracking. The small drift cells, designed for fast response and better position measurements, reduce the number of clusters which can be collected by one wire and increase the fluctuation. Besides, the COT runs at 1 atm, a much lower pressure than the drift chambers which are optimized for dE/dx measurement. Therefore, the resolution of the COT dE/dx is not as high as in Figure 2. A scatter plot will not give us good distinction of particles. To make use of dE/dx from the COT, a plot of mean dE/dx as a function of $\beta\gamma$ is prepared using different particle species. This curve is fitted with an empirical formula [6], the so-called "*universal*" curve.

$$\frac{dE}{dx} = \frac{c_1 \log \frac{\beta\gamma}{\beta\gamma + b} + c_0}{\beta^2} + a_1(\beta - 1) + a_2(\beta - 1)^2 \tag{2}$$

In this equation, c_0, c_1, b, a_1 and a_2 are derived from the fit of data. With this fitted curve, we can predict a particle dE/dx for a given momentum and a mass hypothesis.

By comparing the measured and the predicted value, we can assign probabilities of particle identification and pick the particle type which gives the highest probability.

2.2 COT Electronics

The COT sense wires collect the charge ionized by the incident charged particle and are read out by the ASDQ front-end electronics. The analog signal arrives at the ASDQ and the output is a digital pulse. The leading edge gives the arrival time information and the pulse width is related to the amount of charge collected by the wire. This pulse is sent to the TDC. See Fig. 3 for the COT readout chain.

The ASDQ also provides external controls to turn on and off the dE/dx measurement. When the luminosity is high, the dE/dx measurement can be turned off and the digital pulse width is reduced to avoid the deterioration of two-track resolution. Another control voltage, QDR, allows us to vary the slope of dE/dx versus digital pulse width. Currently the QDR value is chosen so that we can approximate the function width(Q) with a straight line: $y = ax + b$. An internal calibration circuit inside the ASDQ is used to perform calibration of leading edge time and width for all 30240 channels. Two control signals , TREFE and TREFO, vary the amount of charge injected into the pre-amplifier from the calibration circuit.

2.3 Truncated Mean

The amount of charge due to the ionization in the drift chamber has a very broad distribution. The number of clusters created along the path of the charged particle follows Poisson statistics, but the number of electrons in a cluster, which is related to the energy transfer, has a long tail. When the possible energy transfer exceeds the highest atomic binding energy, the fast charged particle undergoes elastic scattering on the atomic electrons as if they were free electrons. The differential energy transfer cross-section per electron becomes the differential cross-section for Rutherford scattering on one electron[1], and the mean transferred energy per collision has a logarithmic divergence [1].

To reach the required accuracy, a track has to be measured on many segments. There are 96 sense wires in the COT. These 96 sense wire layers represent 96 samples of energy loss from 96 track segments. If the segment length is the same for each sample, then measuring the amount of collected charge is equivalent to measuring dE/dx. Since the amount of charge is encoded in the width of the ASDQ output pulse, dE/dx is measured in units of ns. To get the dE/dx of a single track, simply averaging the charge measured from 96 wires will give us a big fluctuation from track to track due to the long tail of the ionization electron distribution. This long tail makes it hard to get a finite mean or variance of the ionization distribution.

[1]proportional to $1/E^2$

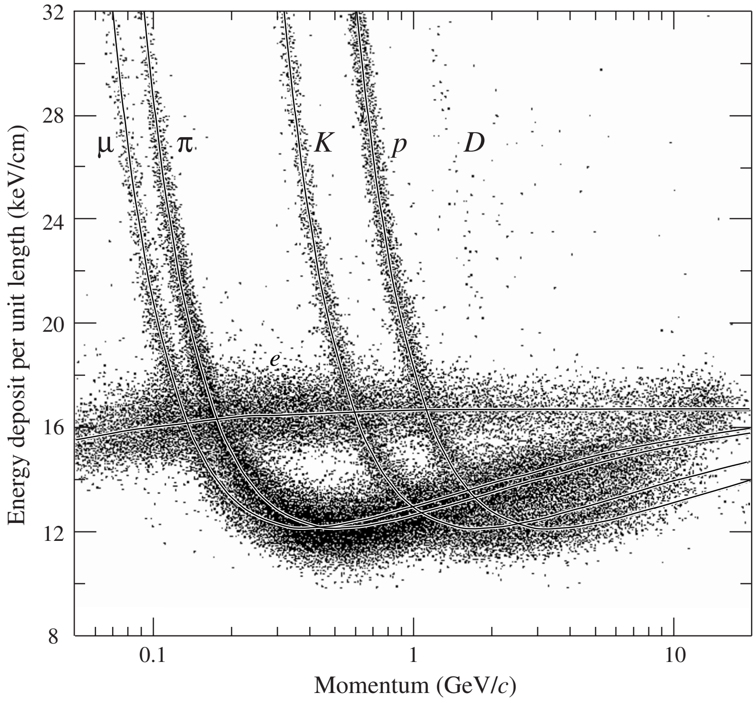

Figure 2: dE/dx as a function of the particle momentum [2]. At low $\beta\gamma$, dE/dx can be modeled by classical physics. The electromagnetic force is only significant within a range r_0. The more time t the incident particle stays in the range of r_0, the longer electrons in the medium will be accelerated, and the larger the transferred energy will be. Therefore dE/dx falls off as $1/t^2 \propto 1/\beta^2$. At high $\beta\gamma$, the logarithmic term describes the relativistic rise. The electromagnetic field of the traveling particle gets stronger as γ goes up, increasing the excitation and ionization cross-section. On top of that, the maximal possible energy transferred goes up with $\beta\gamma$. The relativistic rise is dampened by the shielding of the incident particle field from the polarization of the medium atoms.

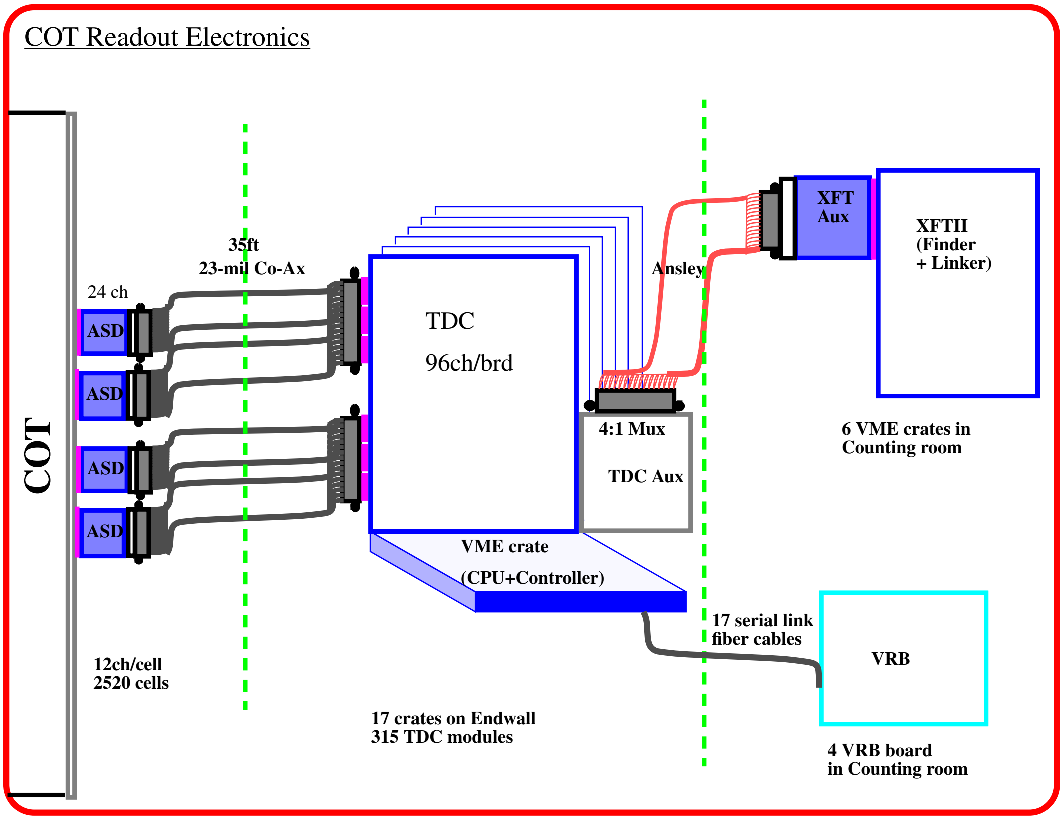

Figure 3: COT Front-end Readout Electronics

Therefore we follow the conventional method: exclude the highest 20% measured values and perform an average over the remaining 80%.

We choose to keep the lowest 80% of measured values based on a study of electron-hadron separation in the lepton+SVT sample by Hung-Chung Fang [7] and our kaon-pion separation in the D^* sample. We first look at electron and hadron (or kaon and pion) dE/dx distributions, and make the areas under the two histograms equal by scaling one of them (see Figure 4 [7] and Figure 29). We compute the overlap region as a percentage of the sum of the two histograms. See Table 1 and Table 2 for the results. We can see the overlap region drops more significantly when truncation decreases from 90% to 80%. We decide to use 80% as a starting point, but more study shall be employed to get the optimal truncation which gives the best separation between electrons, pions, protons and kaons.

Truncation	Overlap region
90%	28.4%
80%	24.1%
70%	22.3%
60%	21.7%

Table 1: *dE/dx separation between electrons (> 4 GeV/c) and hadrons (> 2 GeV/c) in the lepton + SVT sample.*

Truncation	Overlap region
90%	31.9%
80%	29.8%
70%	29.2%
60%	28.8%

Table 2: *dE/dx separation between K and π for $p > 2$ GeV/c in D^* sample*

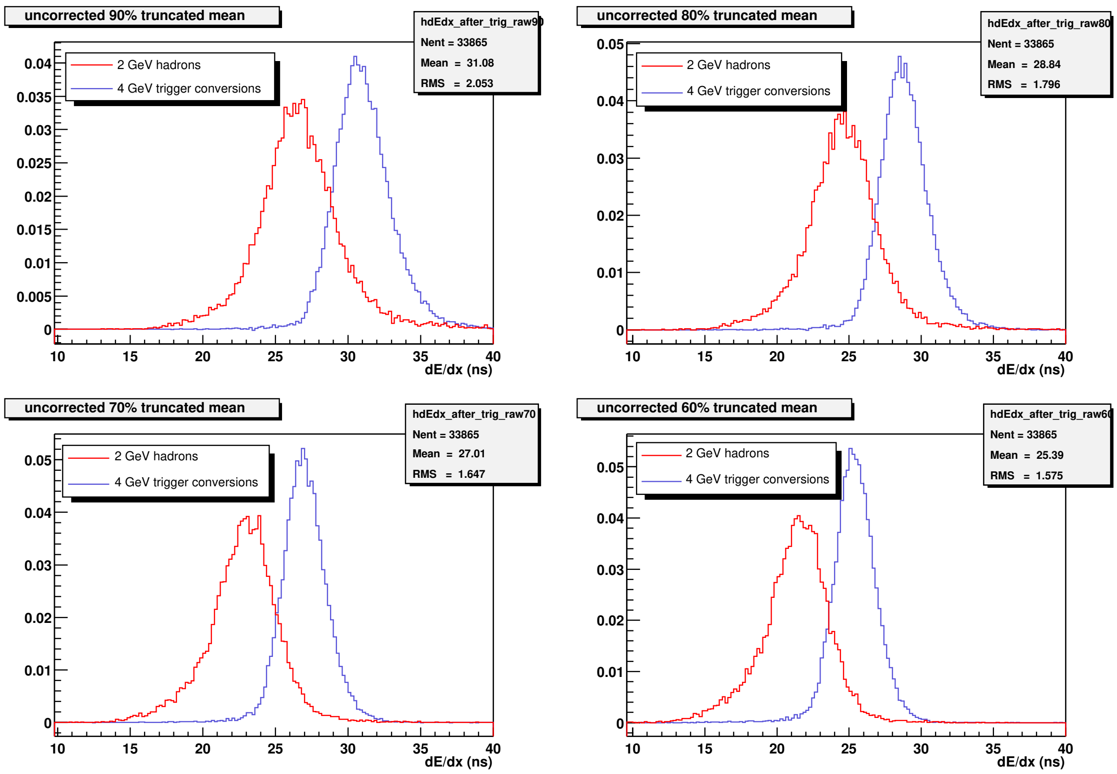

Figure 4: Hung-Chung Fang's study of electron ($> 4\ GeV/c$) and hadron ($> 2\ GeV/c$) dE/dx separation in lepton+SVT samples

3 Sample Selections

Conversion electrons are chosen to study the dE/dx dependence on the drift chamber or cell conditions for two main reasons. First, clean conversion electrons can be obtained by cutting on the $\cot\theta$ difference of two tracks. Second, electron dE/dx is independent of the momentum for momentum greater than 0.4 GeV/c (see Figure 2). High P_T electrons from the W and Z decays are used to cross-check the removal of superlayer and wire dependence after applying 2D aspect angle and drift distance tabular correction. Minimum Bias data is used to study dE/dx dependence on the COT sense wire high voltage. In the following subsections, the cuts applied to select these samples are listed.

3.1 Conversion Electrons

Conversion electrons are reconstructed from the 4.3.1 stripped dataset id jbot4e (this id now is not conversion electron dataset) from runs 139384 through 145046. We look for the all the CdfEmObjects in the event which pass the following cuts:

- $P_T > 4$ GeV$/c$
- $E_T > 4$ GeV$/c^2$
- $E_{had}/E_{em} < 0.125$

Then we loop over all the COT tracks and look for the conversion partner to the CdfEmObject. The partner track shall pass the following cuts:

- $|\Delta\cot\theta| < 0.15$
- $Sep_{xy} < 0.5cm$

Here $\Delta\cot\theta$ is the $\cot\theta$ difference between the two tracks, and Sep_{xy} is the separation at the point when the trajectories of two tracks are parallel on the R-ϕ plane. Finally we use CTVMFT to get the precise conversion vertex position and apply the following cuts:

- $0 <$ conversion radius < 35 cm
- The z difference of two tracks at the vertex < 2 cm

The goal of the first cut is to avoid using the electrons from the conversion at COT inner wall [2]or inside COT. This type of conversions tend to have two tracks sharing one hit at a superlayer and the dE/dx of this hit will be overestimated. See Figure 5.

[2]COT inner wall radius is 40 cm

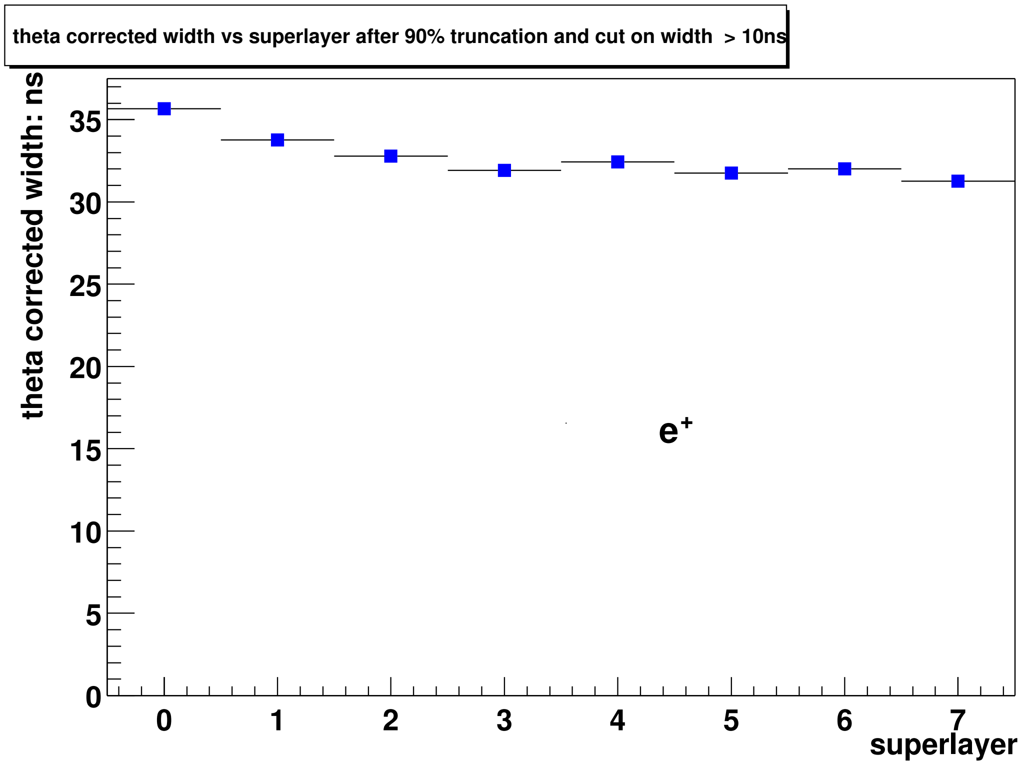

Figure 5: When selecting conversion electrons with conversion radius 0 to 45 cm, superlayer 1 raw dE/dx is higher than the other superlayers due to the hit merging of two tracks close to each other. If selecting conversion electrons with conversion radius 0 to 35 cm, superlayer 1 raw dE/dx will be lower than other superlayers since its sense wires are set at lower voltages. See Figure 20 and Figure 21.

3.2 High P_T Electrons

High P_T electrons from W and Z decays are reconstructed from the 4.3.1 stripped dataset from runs 139384 through 145200. We look for the all the CdfEmObjects in the event which pass the following cuts:

- $P_T > 8$ GeV$/c$
- $E_T > 8$ GeV$/c^2$
- $E_{had}/E_{em} < 0.125$
- $|d_0| < 1$

Then we find the one that has the highest P_T in each event. These high P_T electron tracks were used to check the dE/dx dependence on superlayer and wire before and after the correction. See Section 4.7.2 and Section 4.7.1 for more details.

3.3 Minimum Bias Data for High Voltage Correction

We scanned high voltage for two hours on June 18th, 2002. The high voltage settings for each run are described in Table 3. The trigger table MINIMUM_BIAS_1 was chosen to get the maximum available tracks in a short amount of time. To decouple the aspect angle effect from the high voltage effect, to avoid tracks being cut off by the field sheet and to reduce split pulses, we apply the following cuts on the hits:

- $|\sin\alpha - 0.08| < 0.1$ (See Section 1 for the definition of α.)
- 0.3 cm < drift distance < 0.5 cm
- not from the end wires, only use hits from wire 1 to 10

Then, in each bin of high voltage, hits are sorted according to the value of dE/dx, and only the lowest 90% are kept.

We used physics dataset 'iphysr' of runs 146766 through 146768. For more details about high voltage correction, see Section 4.5

Run	High voltage (% of the normal settings)
146766	100%
146767	98%, 96%, 94%, 92%, 91%, 93%
146768	93%, 95%, 97%, 99%, 100%

Table 3: *High voltage settings in each run during the test on June 18th, 2002*

4 dE/dx Correction

4.1 Introduction

Theoretically, dE/dx is only a function of the particle's velocity and the global drift chamber properties. Experimentally, dE/dx depends on several local properties of the drift chamber, such as high voltage for each superlayer or wire location in a cell, and also on the characteristics of tracks and hits, such as dip angle θ, p_T, aspect angle and drift distance. All these dependence have to be removed.

Most of the corrections presented are done on hit width, i.e. the individual charge measurement. The exception is the global pressure correction. Since the pressure change will affect the gain of the whole chamber, this correction is applied on the 80% truncated mean width.

To give readers an overview of the dE/dx corrections, all the corrections applied are listed first. More details will be presented in the subsections.

- merging of hit widths for split pulses
- electronics pedestal subtraction
- θ (dip angle) correction
- high voltage correction
- hit z position correction
- aspect angle and drift distance correction
- pressure correction

4.2 Merging of Hit Widths for Split Pulses

Split pulses come from the clusters (on the same segment) which arrive at the sense wire at different times. See Figure 6 from [3] for the drift time simulation with Garfield. When a track segment is close to the sense wire, it passes more isochrones than when far away. The arrival times of the clusters on the segment are more dispersed. Some clusters might arrive later than others. The arrival time difference lets the input charge of the ASDQ fall below the discriminator threshold for a few ns and come above the threshold at a later time; therefore more than one pulse is induced by a single track segment. See Figure 7 for an example output of the ASDQ. Offline tracking picks up the earliest hit that triggers the electronics and matches the t_0. The energy loss of this track segment is underestimated if we only calculate dE/dx with the hit used by tracking. We correct this effect by adding the width of split pulses.

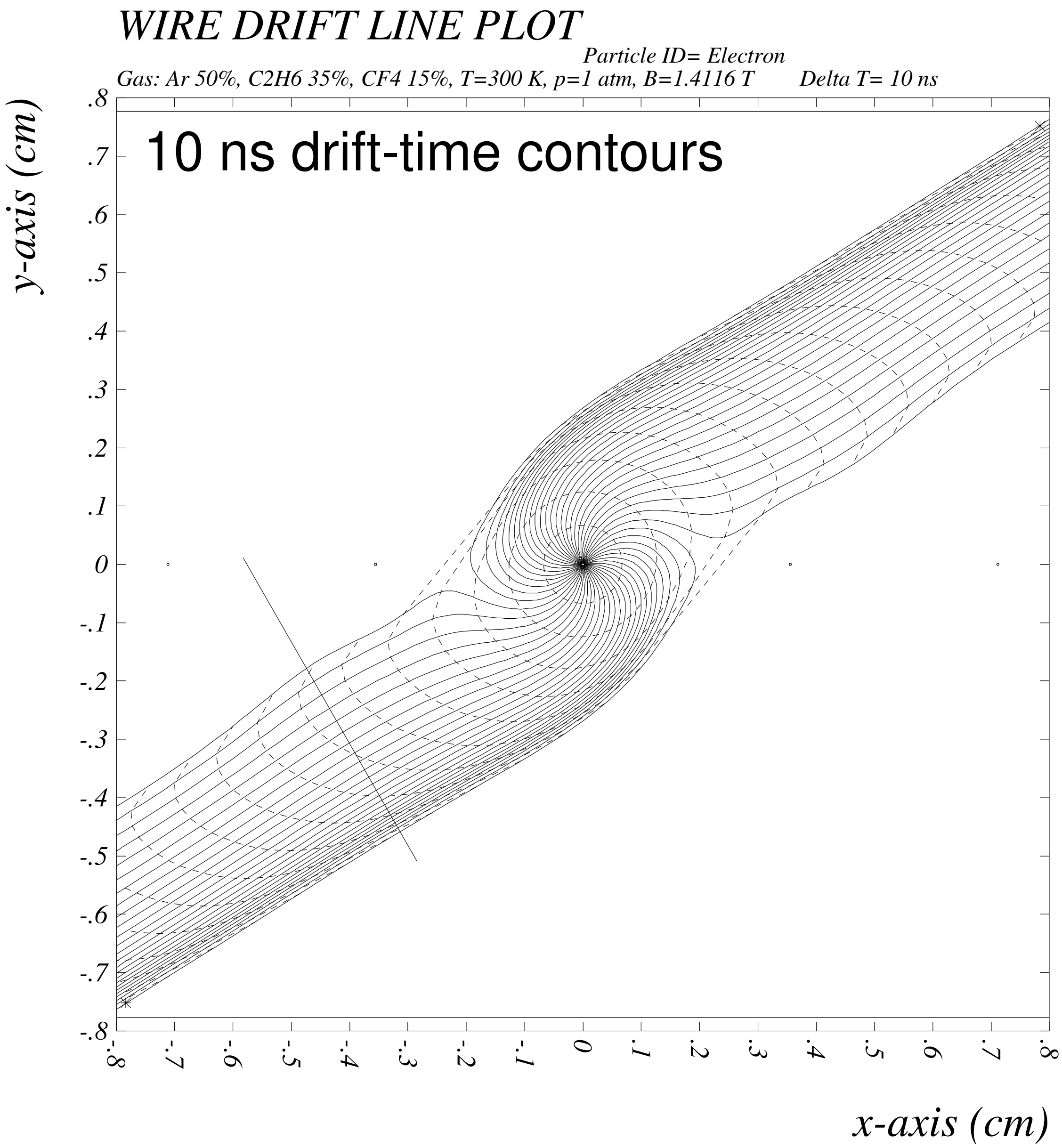

Figure 6: Drift-lines (solid) and isochrones (dashed) for simulated (GARFIELD) COT cell. Time contours at 10 ns intervals. The location of the typical track is shown.

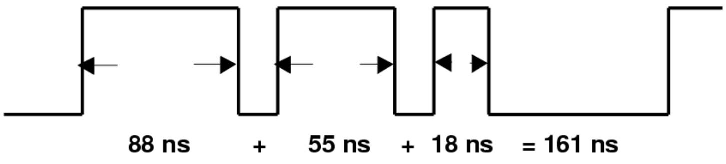

Figure 7: An example of a series of split pulses. The width of each pulse is summed up to give a final measurement of hit width.

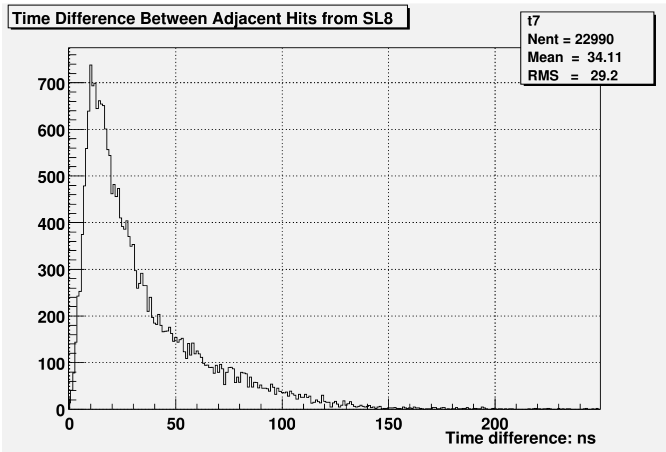

Figure 8: Time difference distribution between any adjacent hits on the wires in superlayer 8. The distribution peaks at 15 ns. We define the hits which are less than 15 ns away as split pulses.

To decide when we shall consider that two adjacent hits on the same wire come from the clusters on the same segment, or come from two different tracks, we look at the distribution of the arrival time difference between any adjacent hits on one wire. Figure 8 shows that the time difference peaks at 15 ns. We decide to define any hits that are less than 15 ns away from each other as partners.

After we define the criteria, we can look at the drift distance distribution for the hits which have at least one partner. As we expected, there are at least a factor of two more split pulses in the small drift distance region (when the hits are close to the wire) than the normal drift distance region. See Figure 9.

We merge the hits that are less than 15 ns away from each other by adding their hit widths. If the earliest hit in the group is not picked up by the pattern recognition and used in the tracking, we reject the group. See Figure 10 for a comparison of the dE/dx before and after merging the hit width of split pulses. The operation does decrease the dip region by 1 ns.

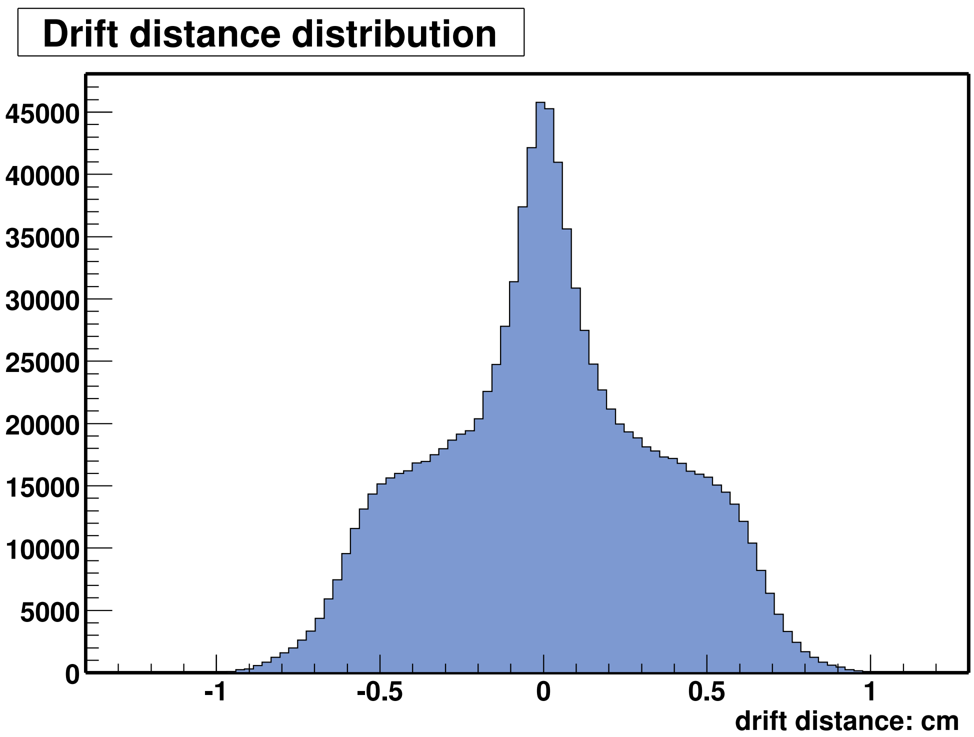

Figure 9: Drift distance distribution from the hits that have at least one hit less than 15 ns away from them on the same wire. The number of split pulses in the region (drift distance < 0.1 cm) is a factor of 2 more than the number in the region (drift distance > 0.3 cm).

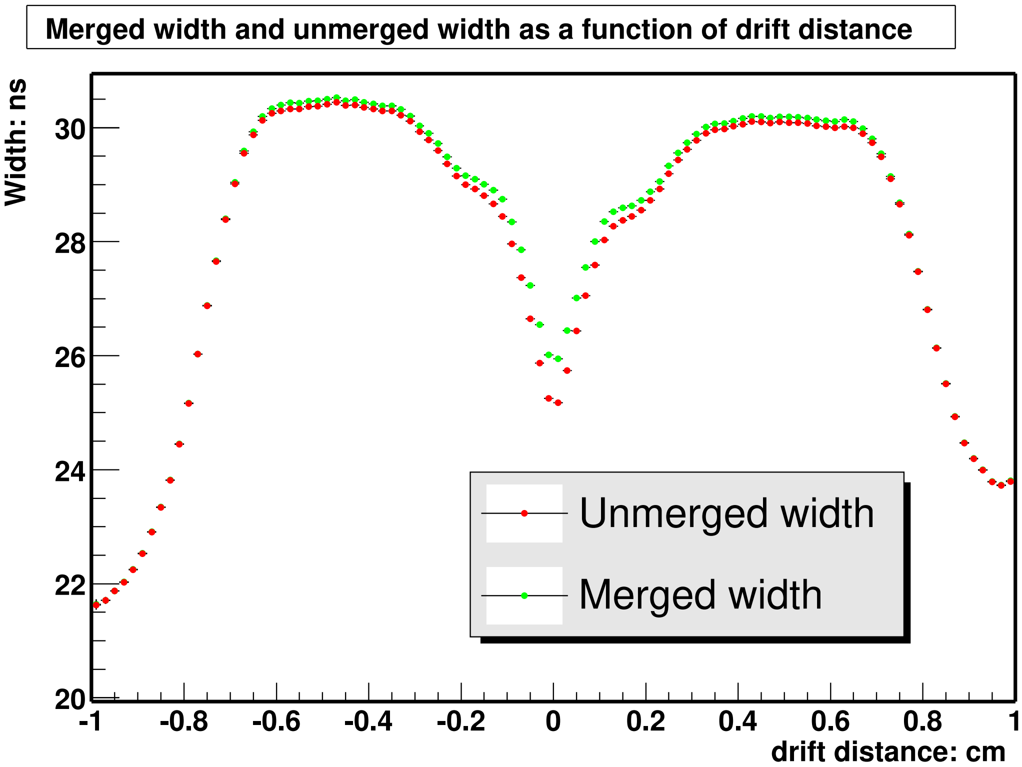

Figure 10: A comparison of the dE/dx as a function of drift distance before and after merging the hit widths of split pulses. dE/dx does not depend on the drift distance when the ionization occurs at the central region of a drift cell. In the plot, dE/dx is a constant in the region: 0.3 cm $<$ drift distance $<$ 0.5 cm. When drift distance gets shorter, dE/dx decreases as there are more split pulses. When the drift distance gets longer, i.e. the ionization occurs very close to the field sheet, part of the clusters on the track segment will be collected by other wires. dE/dx drops significantly at the cell boundary. As shown in the plot, after merging the hit width, the small dip in the region:drift distance $<$ 0.1 cm is decreased by 1 ns.

4.3 Determining Electronics Pedestal

The digital pulse width is not a linear function of the charge, i.e. when the width is zero, the amount of charge is not zero. After adding the width of split pulses, we subtract the electronics pedestal from the sum. To get the pedestal, first we use the conversion electron sample to plot the hit width as a function of $\frac{1}{\sin\theta}$, a quantity that is proportional to the 3D path length of the charged particle . For electron $P_T > 2$ GeV/c, particle trajectory in the $r-\phi$ plane is a straight line and the 2D path length, $L_{r\phi}$, is simply the inner and outer radii difference of COT. The 3D path length, L, is $L_{r\phi}/\sin\theta$. Electron dE/dx is also independent of the momentum in this region, therefore

$$charge\ q = a \times dE/dx \times L = a' \times L,\ L \propto \frac{1}{\sin\theta} \tag{3}$$

Here a is a constant that depends on the gas. Now using the first order approximation, we assume the relationship between the charge and the width can be described as a straight line of the form.

$$width = F(q) = a_0 \times q + a_1 = a_0' \times \frac{1}{\sin\theta} + a_1 \tag{4}$$

We find $a_1 = 12$ ns after fitting Figure 11 with a straight line. Each correction after this was done on (hit width - 12 ns), instead of hit width. First we fit (hit width - 12 ns) as a function of one specific variable, for example, COT high voltage. Then we choose a reference point and use the fitted formula to calculate a correction factor. By multiplying each hit width with the correction factor, we move every hit width to the reference point.

4.4 θ Correction

Tracks traverse the cells at different angles θ with respect to the beam line (z direction). See Figure 12. When a track has larger θ, its path length is shorter. The ones of shortest path length are the tracks whose θ equals 90^0 . The larger the path length is, the more energy loss the incident particle can have. To properly interpret the measured amount of charge, Q, as dE/dx, we have to make the path length of each hit equal. Here the reference point is the dE/dx at $\theta = 90^0$.

The fitted formula for runs 139390 through 143300 is given by

$$\frac{dE}{dx} = c0 \times (1 + (1.350 \pm 0.006) \times \ln(\frac{1}{\sin\theta})) \tag{5}$$

Therefore the correction factor we obtain is $(1 + (1.350 \pm 0.006) \times \ln(\frac{1}{\sin\theta}))$ for θ correction.

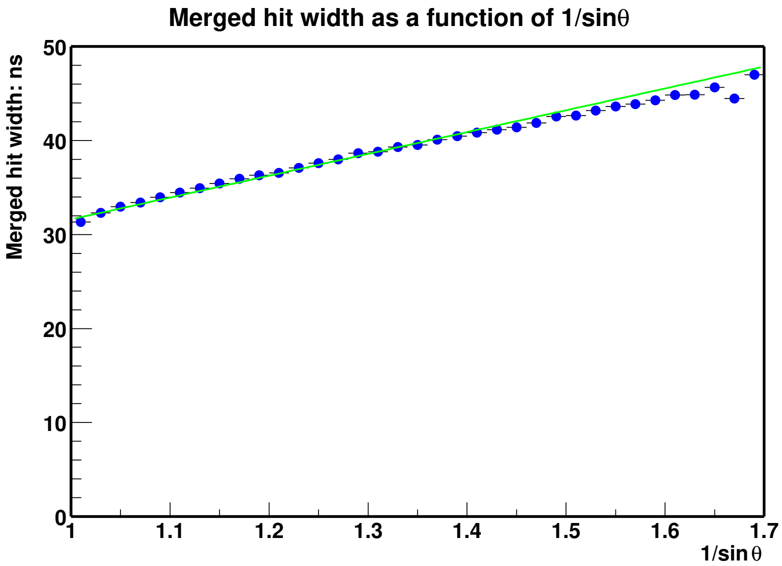

Figure 11: dE/dx pedestal is defined as the width when $1/\sin\theta = 0$. The electrons from W and Z decays were used for runs 139390 through 143300.

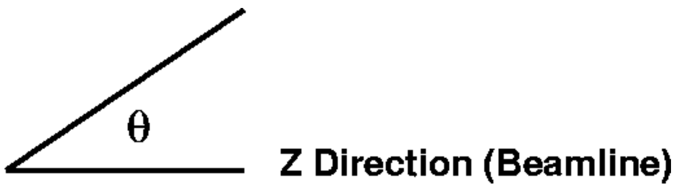

Figure 12: A track observed in the rz plane.

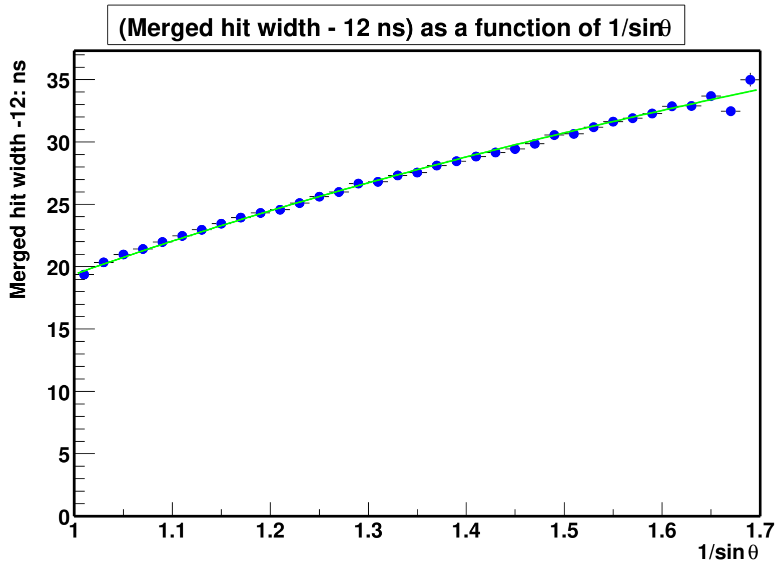

Figure 13: dE/dx θ calibration using conversion electrons for runs 139390 through 143300.

4.5 High Voltage Correction

Each superlayer has a different gain since the inner layers are more likely to trip and therefore are kept at a lower voltage than the others. For example, before run 143809, superlayer 1 has been kept at 100% of the designed settings[3] for the stability of the drift field, while others have been kept at 101.5%. [4]

From runs 143809 through 144623 the high voltage at superlayer 3 tripped frequently. After finding a broken wire and disabling cell 2, the whole superlayer 3 is kept at 100% too. Quadrant A and D of Superlayers 2 tripped several times but were fixed and recovered. The whole superlayer 2 is still kept at 101.5% of the nominal setting. For the period when only one quadrant of one superlayer is at the abnormal setting, hits from this quadrant are ignored and will not contribute to the track dE/dx calculation.

The high voltage correction factor cannot be computed through the data from the physics runs. First of all, there are not enough high voltage variations for every

[3]The high voltage on each sense and potential wire is calculated based on a Garfield simulation. [10] The goal is to achieve a gain of 2×10^4 and to minimize the difference of space-drift-time relations and drift fields between different superlayers, middle wires and end wires.

[4]We run high voltage at 101.5% of the designed settings for most superlayers instead of 100% based on a single wire efficiency study. While running high voltage at 100% with the ASDQ threshold at 225 to 250 mV, we have 3 to 4.6 % missing hits on the tracks with $P_T > 1$ GeV/c and traversing all 8 superlayers. While running at 101.5%, there are 1.2% missing hits. Now the current high voltage configuration gives us 98 to 99 % single wire efficiency. [11]

superlayer.[5] Secondly, these runs are usually long and span over 24 hours; the pressure dependence can come into play. To minimize the pressure fluctuation, we took around 2 hours of data and varied the high voltage from 101.5% to 92.4% for superlayer 2 and 4 to 8, 100% to 91% for superlayer 1 and 3. See Section 3.3 for the sample selection criteria.

See a result of the scan from Figure 14 and the fluctuation of the parameters fit from superlayer to superlayer in Figure 15. Each curve can be fitted with an exponential function (see Equation 6). We choose 101.5% as the reference point since most superlayers are run at this voltage. As one can see, the fitted constants for 0th order are not the same for every superlayer; this difference will be handled in the aspect angle and drift distance 2D look-up tables. The correction factor we obtain for high voltage correction is $\exp((V/101.5-1)\times p1)$.

$$\frac{dE}{dx}_{\theta corrected} = p0 \times \exp((V/101.5-1)\times p1) \tag{6}$$

The high voltage values might change in the future as well. Now the values are stored in the database with table id 'COTHV'. Every change of high voltage state is a new entry in the table. The variables in the table are as follows:

- lineIndex: a number only for the database use
- beginRun: the first run when the high voltage state changes
- normalFlag: a flag which indicates if the high voltage is at a normal state: Superlayer 1 at 100% of the nominal setting, other layers at 101.5%
- ignoreRunFlag: a flag which indicates if this run shall be ignored and dE/dx will not be calculated. A QDR or HV test run always have this flag turned on.
- superLayer: the superlayer number that has its HV different from the normal state
- startCell: the first cell number that has its HV different from the normal state
- endCell: the last cell number that has its HV different from the normal state
- startWire: the first wire number that has its HV different from the normal state
- endWire: the last wire number that has its HV different from the normal state
- highVoltage: the high voltage setting in % of the nominal setting. If only part of the cells are ignored, the ignoreRunFlag will be off, and this variable will be -1.

[5] There are only two data points available for comparison: 101.5% and 100% of the nominal settings for superlayer 3.

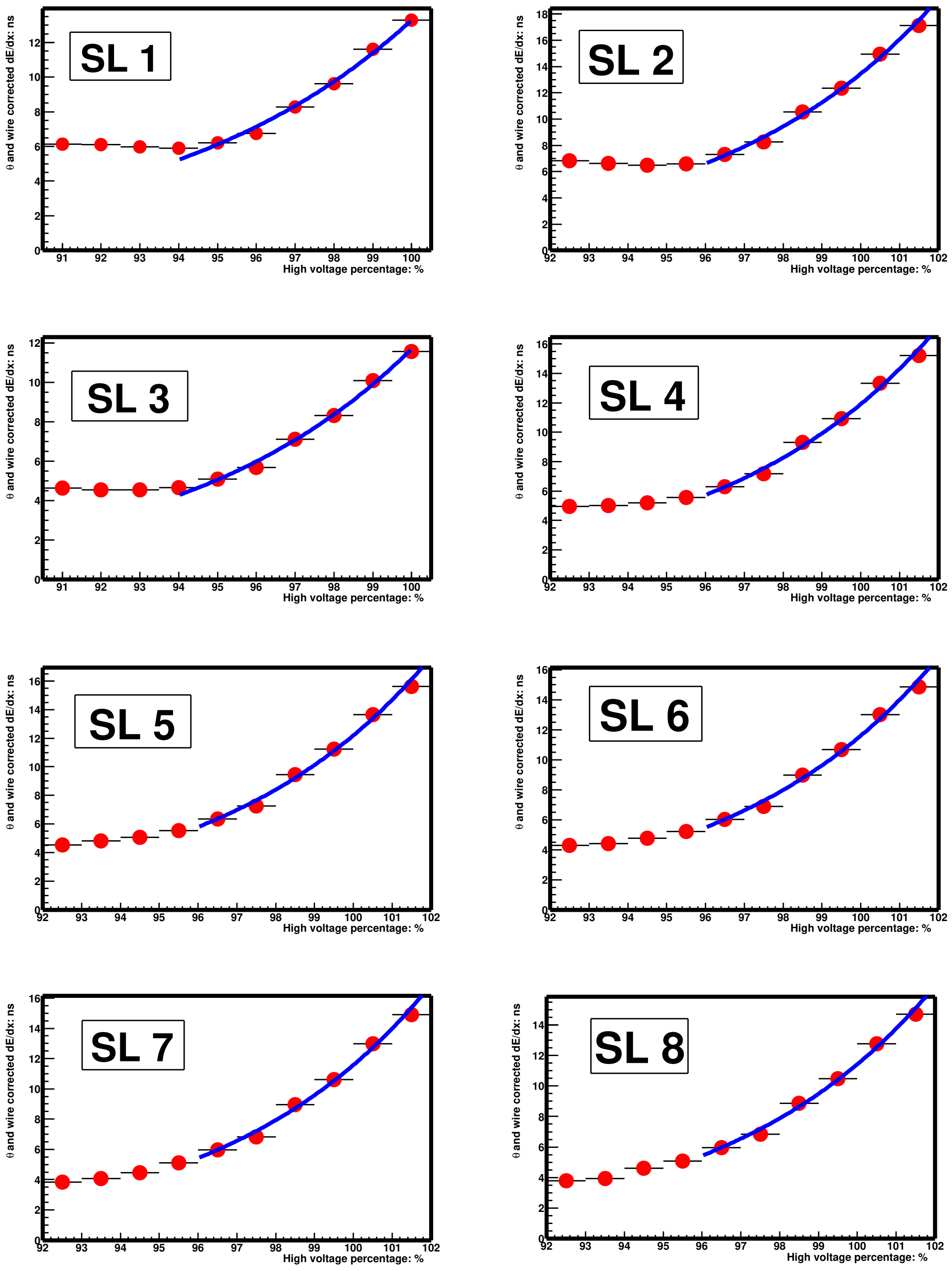

Figure 14: Uncorrected dE/dx as a function of 10 high voltage settings for each superlayer. Used all the tracks in each event from trigger MINIMUM_BIAS with some quality cuts, Run number is 146767. Note: for high voltage below 94%, the gain is so low that the ASDQ digital pulse width has reached its minimum and can not go lower. So these points can not be included in the fit.

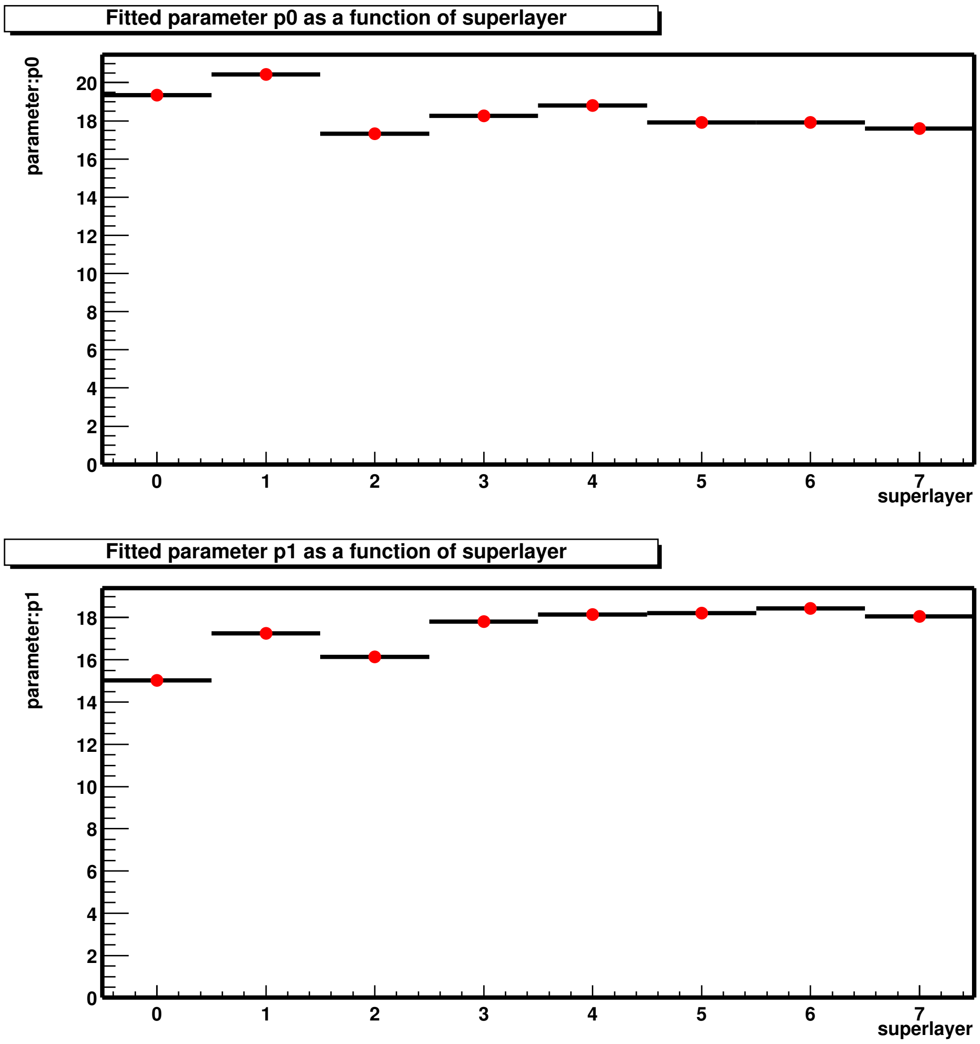

Figure 15: The fitted parameters of Equation 6, $p0$ and $p1$, as a function of 8 superlayers.

4.6 Hit Z Position Correction

The digital pulse width of the ASDQ can also depend on the hit z position on the wire. Since we read out the signal from only one end of the wires, there is small signal attenuation as the signal travels down from the point where the charges are collected to the ASDQ readout end. Superlayer 1, 4, 5 and 8 are readout at the +z end while the others are readout at the -z end. We make this correction for each superlayer. See Figure 16 and Figure 17 for the dE/dx in superlayer 8 before and after the correction. The correction is done by fitting Figure 16 with a straight line and use z=0 as the reference point. The correction factor we obtain has a general form: $(1 + c_0 \times (hit\ z\ position))$.

4.7 Aspect angle and drift distance Correction

When a track segment is close to the field sheet, not all the clusters on that segment will be collected by one wire. Some of them will go to the other cell. The aspect angle of that track segment determines the proportion of the charge which will go to other cell, since the proportion is a function of 'aspect angle $\pm$ Lorentz angle', where $\pm$ depends on the charge of the track.

In addition, Hits of different aspect angle or different drift distances will induce pulses of different shapes due to the complex drift field. These pulses trigger the electronics at different time and the amount of charge integrated will also vary. Hence the final digital output of the ASDQ can have a broad distribution.

dE/dx is a complicated function of these two variables and hard to be parameterized with simple polynomials. The dependence on the aspect angle and drift distance can not be decoupled either. We decide to build two-dimensional look-up tables for 96 layers: one dimension being $\sin\alpha$[6] and the other being the drift distance. The correction factor can be calculated by dividing the truncated mean width in each bin with the width of the reference point.

The reference point is the average dE/dx of all the hits on superlayer 8, wire 1-10[7], whose 0.3 cm $<$ drift distance $<$ 0.5 cm and $|\sin\alpha - 0.08| < 0.1$. There are 10 bins in the $\sin\alpha$ dimension and 20 bins in the drift distance dimension. We interpolate the hit correction factor linearly in the $\sin\alpha$ dimension to compensate the big granularity chosen due to small statistics. These 96 tables not only remove the dependence on the drift distance and the aspect angle, but also remove the difference between middle wires and end wires, and the difference between 8 superlayers. See Section 4.7.1 and Section 4.7.2 for a check of the wire, superlayer dependence removal with electrons from W and Z decays.

[6] See Section 1 for the definition of aspect angle α

[7] excluding the two end wires

4.7.1 Wire Dependence

There are 12 sense wires in each cell. The wires at the two ends of the cell will collect more charge than the ones in the middle. The open-cell geometry allows more charge to be deposited at the two end wires in a cell since the charge deposited at the boundary of two superlayers has no place to go but to the end wires.

See Figure 18 and Figure 19 for the uncorrected dE/dx and the dE/dx after 2D look-up table correction.

4.7.2 Superlayer Dependence

As mentioned in Section 4.5, there is still difference of dE/dx between different superlayers. Also each superlayer has different cell sizes which can give different dE/dx especially for the tracks that are close to the field sheet. The tracks which pass by smaller cells have more chance to be clipped by the field sheets. After the 2D look-up table correction, dE/dx is uniform over all the superlayers.

See Figure 20 for the uncorrected dE/dx before run 143300[8], Figure 21 for the uncorrected dE/dx after run 144650[9] and Figure 22 for the dE/dx after 2D look-up table correction.

4.8 Pressure Correction

As the gas pressure of COT increases, the amount of primary ionization increases because the charged particle passes through more medium. However, the mean free path for each electron in the avalanche region is decreased. Before an electron is accelerated long enough to gain sufficient energy to ionize another atom, producing a secondary electron, it has collided with another atom. Thus the overall gain and the total number of electrons collected are reduced. Without any hardware correction, the relative change of pressure will cause a factor of $5 \sim 6$ relative change in the gain [4].

$$\frac{\Delta p}{p} = -5 \sim 6 \frac{\Delta g}{g} \tag{7}$$

Luckily, Aseet Mukherjee devised a feedback circuit which will monitor the pressure change and adjust the high voltage to compensate the gain. After the installation of the feedback circuit, the dependence of pressure is almost negligible.

Conversion samples from runs 144721 through 145200 [10]are used to check the response of pressure. We obtain a correction formula 8 for the residual pressure dependence and Figure 23. In Figure 23, each bin is side-band subtracted with

[8]See the introduction for the high voltage settings at this period

[9]See the introduction for the high voltage settings at this period

[10]We don't have pressure monitor before run 142558

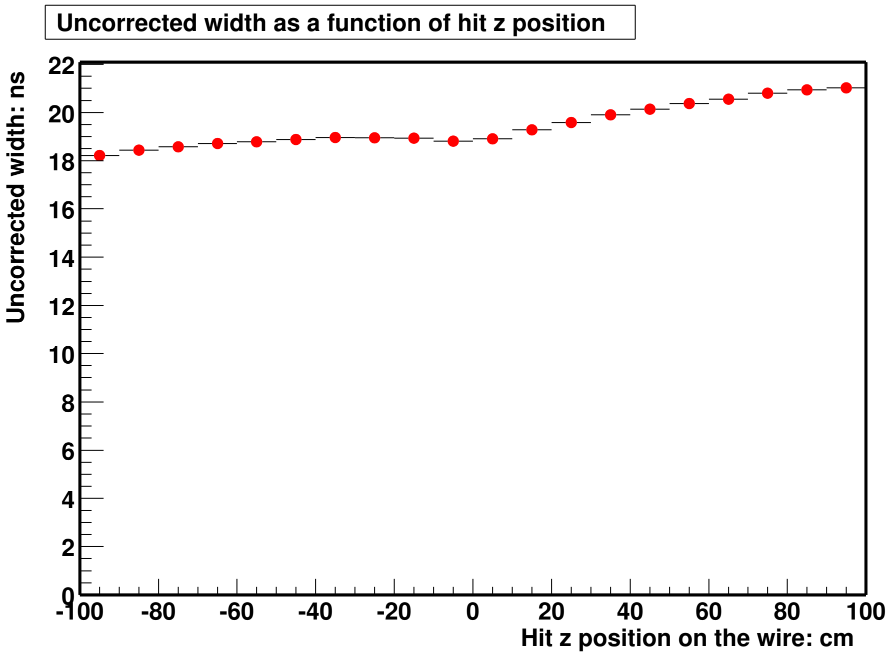

Figure 16: Uncorrected dE/dx as a function of hit z position on the wire, superlayer 8. Use conversion electrons for runs 138612 through 145077.

$\Delta \cot\theta$ distribution. In this conversion sample, S/N is about 22 in the signal region. The correction factor we obtain is $\times(1-(0.1429\pm0.0024)\times(pressure-14.5))$.

$$\theta\ corrected\ width = (19.75\pm0.01)\times(1-(0.1429\pm0.0024)\times(pressure-14.5)) \quad (8)$$

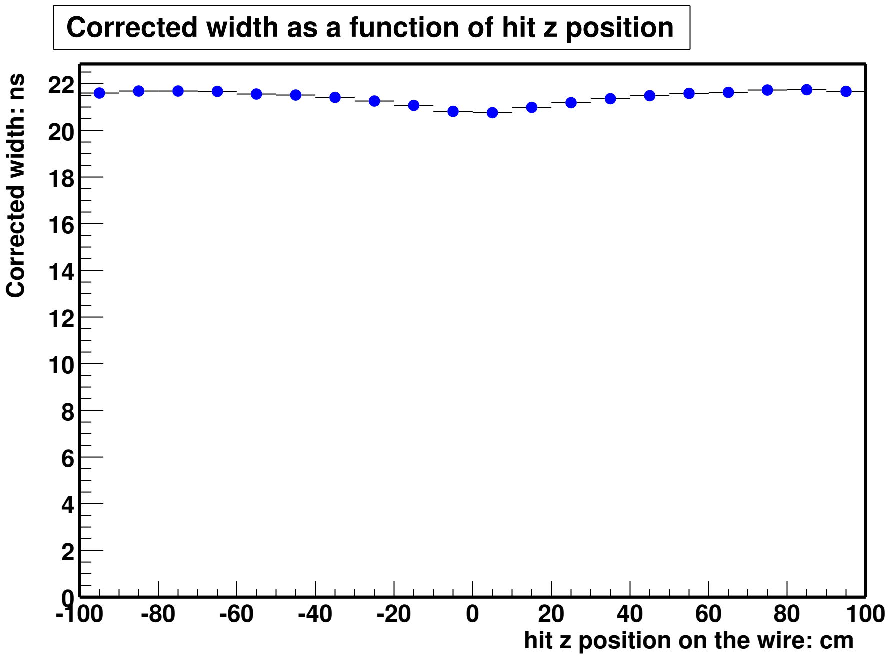

Figure 17: Hit z position corrected dE/dx as a function of hit z position on the wire, superlayer 8. Use conversion electrons for runs 138612 through 145077.

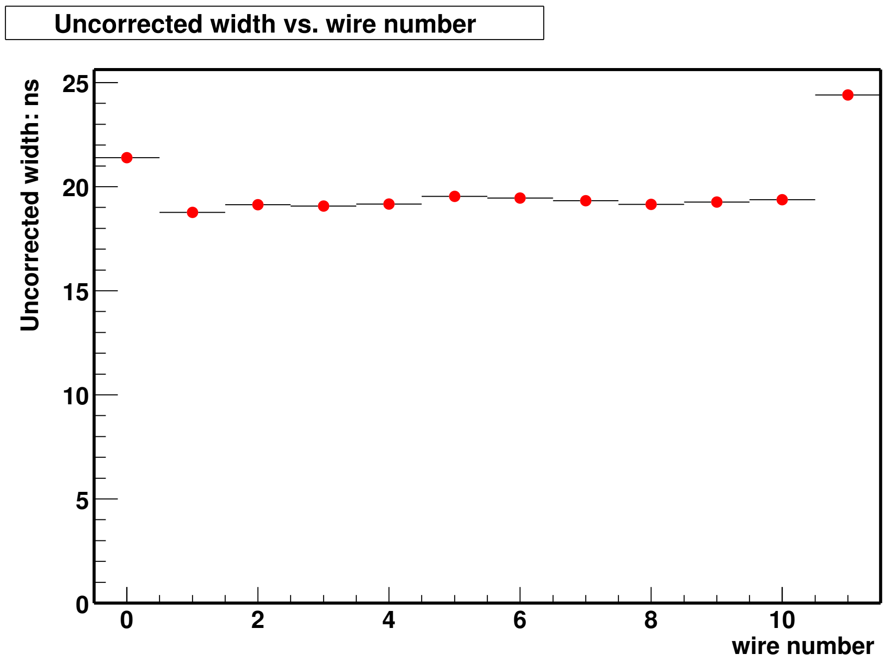

Figure 18: Uncorrected dE/dx as a function of the wire number. Electrons from W and Z decays are used for runs 139384 through 145046.

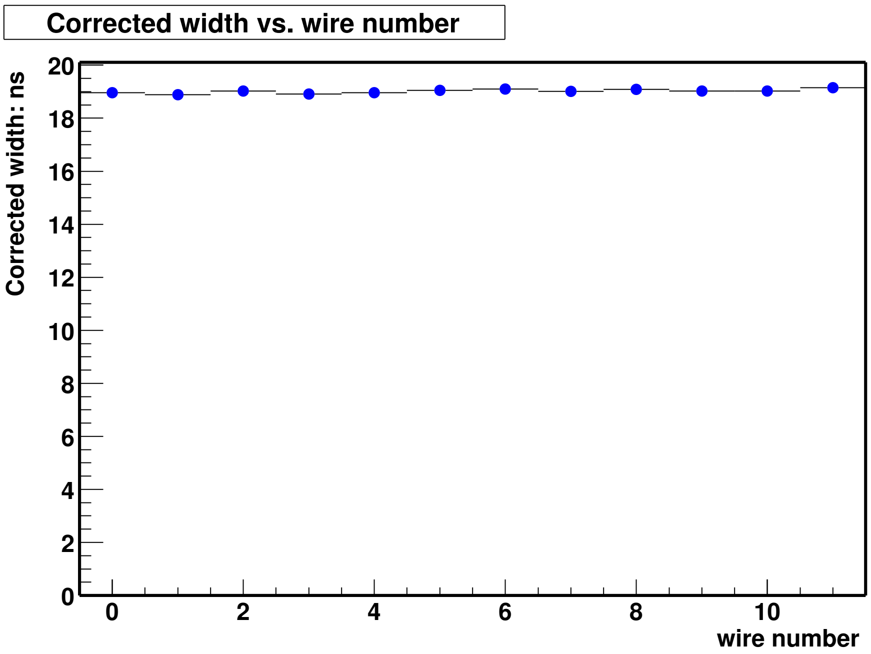

Figure 19: dE/dx as a function of the wire number after applying 2D look-up table correction.

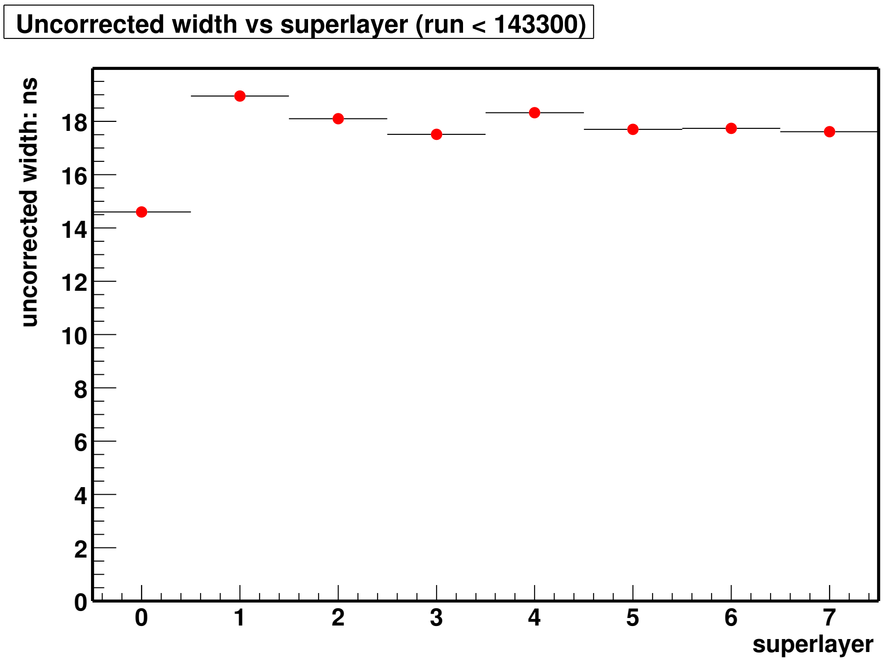

Figure 20: Uncorrected dE/dx a function of 8 superlayers. Electrons from W and Z decays are used for runs 139384 through 143300.

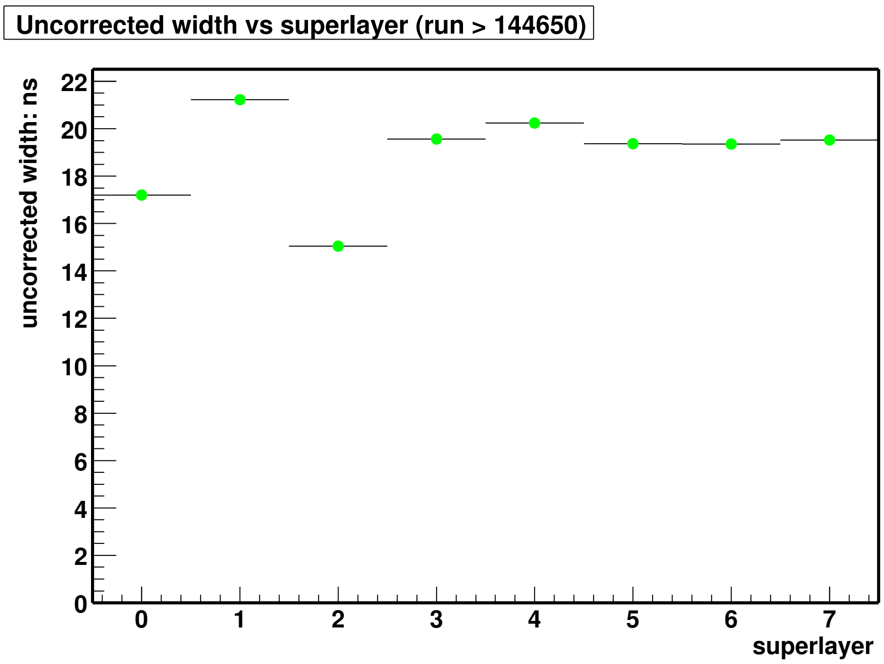

Figure 21: Uncorrected dE/dx as a function of 8 superlayers. Electrons from W and Z decays are used for runs 144650 through 145046.

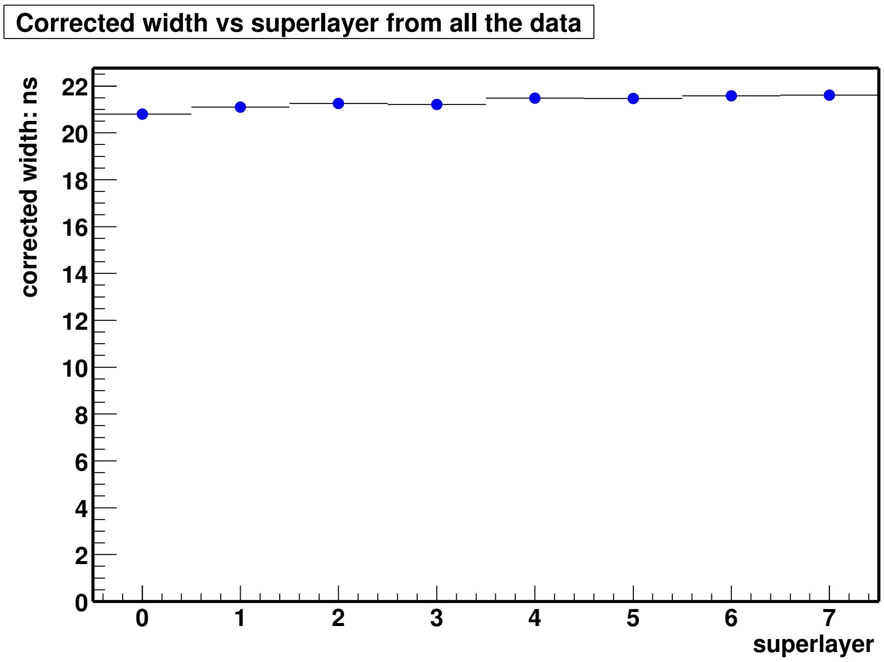

Figure 22: θ, high voltage, wirez and aspect angle, drift distance corrected dE/dx as a function of 8 superlayers, for runs 139383 through 145046.

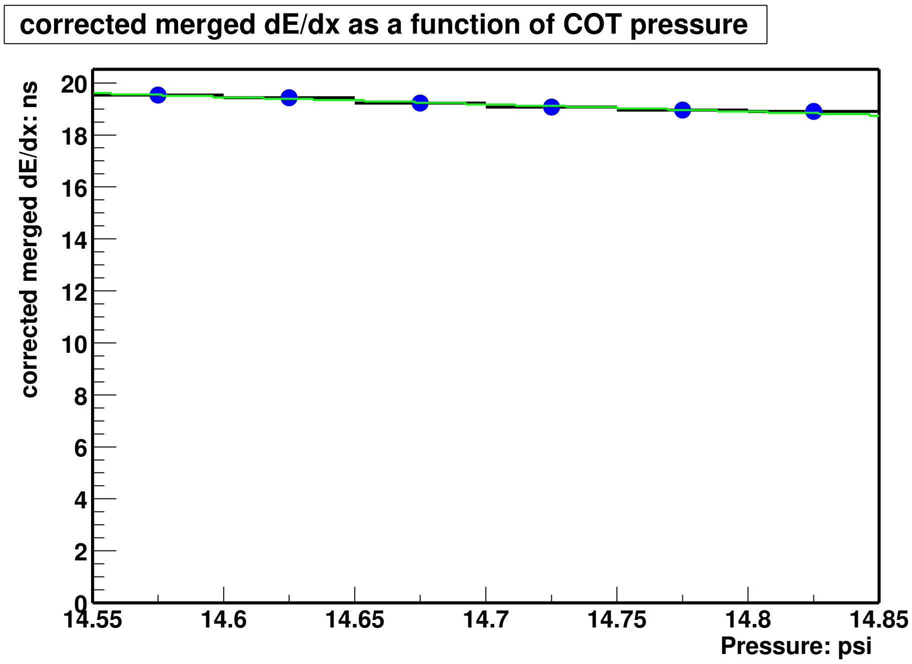

Figure 23: dE/dx pressure calibration using electrons from conversions, for runs 144721 through 145200.

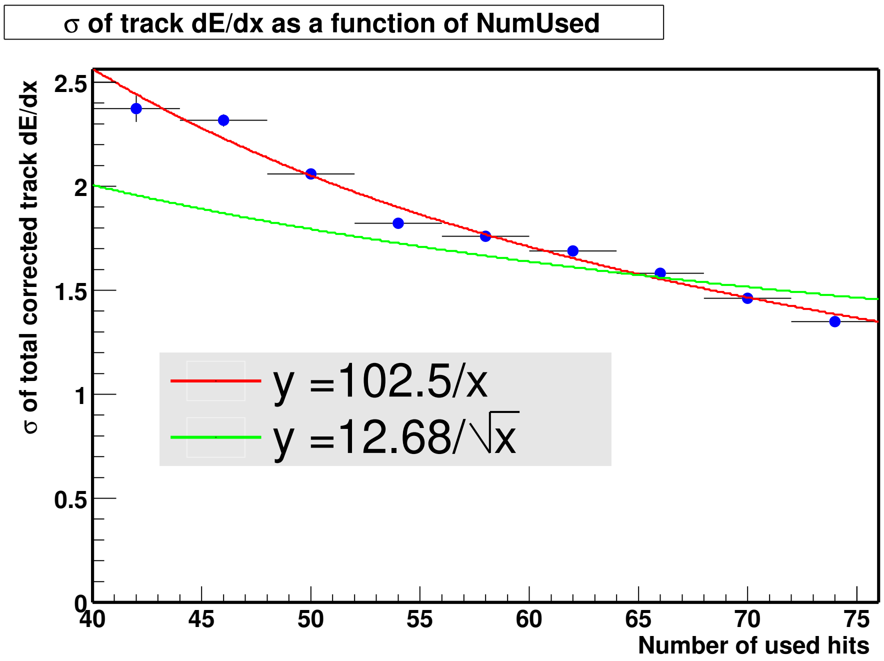

Figure 24: Sigma of dE/dx fitted with two formulas: 1. empirical: $102.5/N_{used}$. 2. conventional (error on the mean): $12.68/\sqrt{N_{used}}$

5 dE/dx Performance

5.1 dE/dx Resolution

Using the conversion electrons, we can establish a formula to describe the resolution of dE/dx as a function of number of the used hits and fit it with Equation 9. As in run I, we can not use the sigma of hit dE/dx [11] divided by $\sqrt{N_{used}}$ (error on the mean) to describe dE/dx's resolution [6]. We can see from Figure 24, $\frac{c0}{\sqrt{N_{used}}}$ underestimates the sigma of dE/dx for $N_{used} < 65$.

$$\boldsymbol{\sigma_{\frac{dE}{dx}} = (102.5 \pm 0.1)/N_{used}} \tag{9}$$

[11] $\sim$ 13ns

5.2 Universal curves

We use clean samples of the conversion electrons, pions from K_s, muons from J/ψ, protons from Λ, low pt protons, pions, kaons with the TOF information and fit their dE/dx with Equation 2. The fitted curve for the positive and the negative charged tracks are different in the dip region. See Figure 25, Figure 26 and Figure 27. The reasons are unknown and much further investigations are required. For the time being, we decide to provide two universal curves in the offline code.

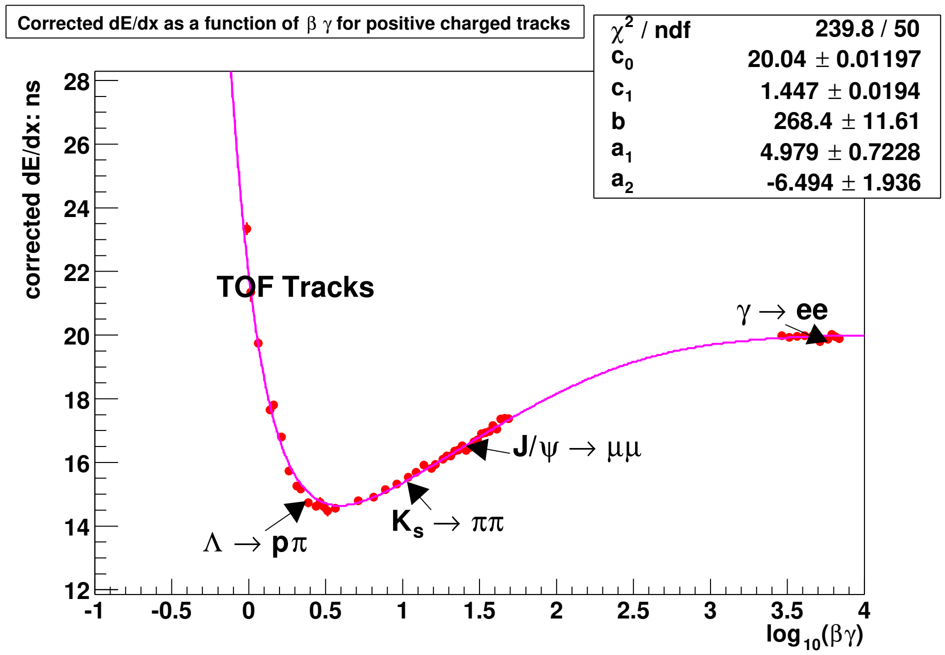

Figure 25: Universal curve for positive charged tracks

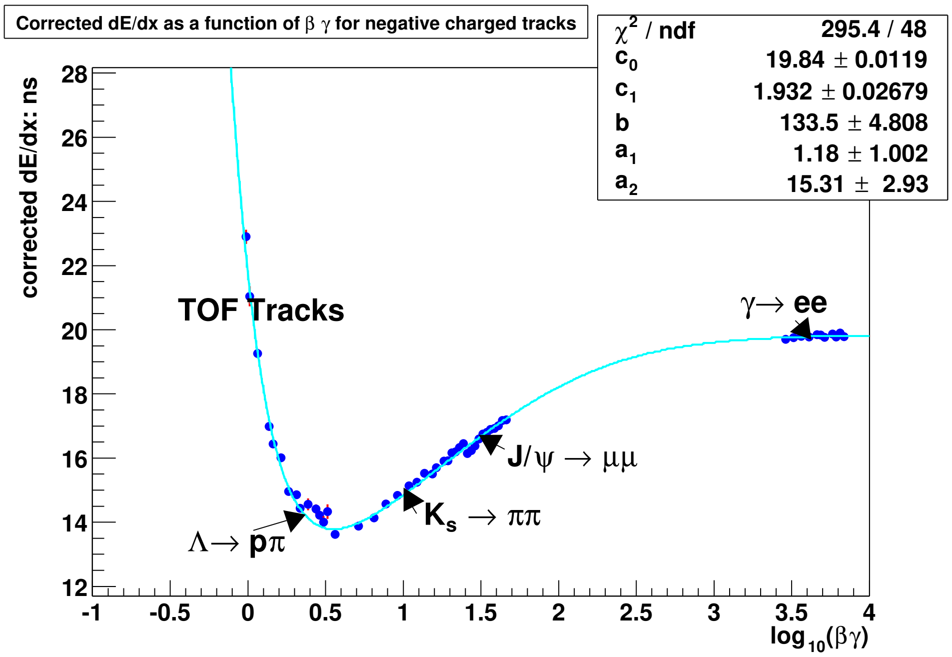

Figure 26: Universal curve for negative charged tracks

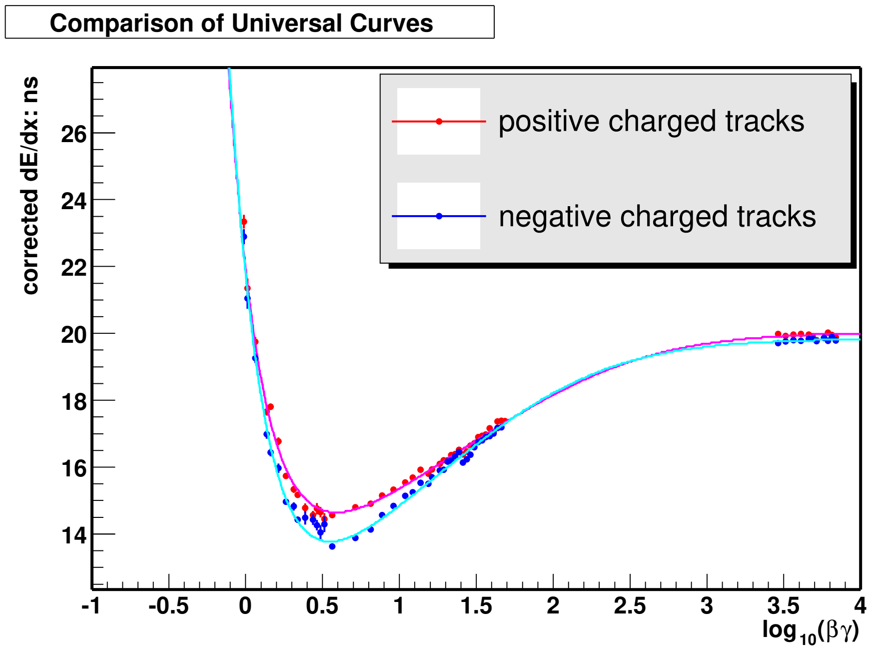

Figure 27: Universal curve comparison for positive and negative charged tracks

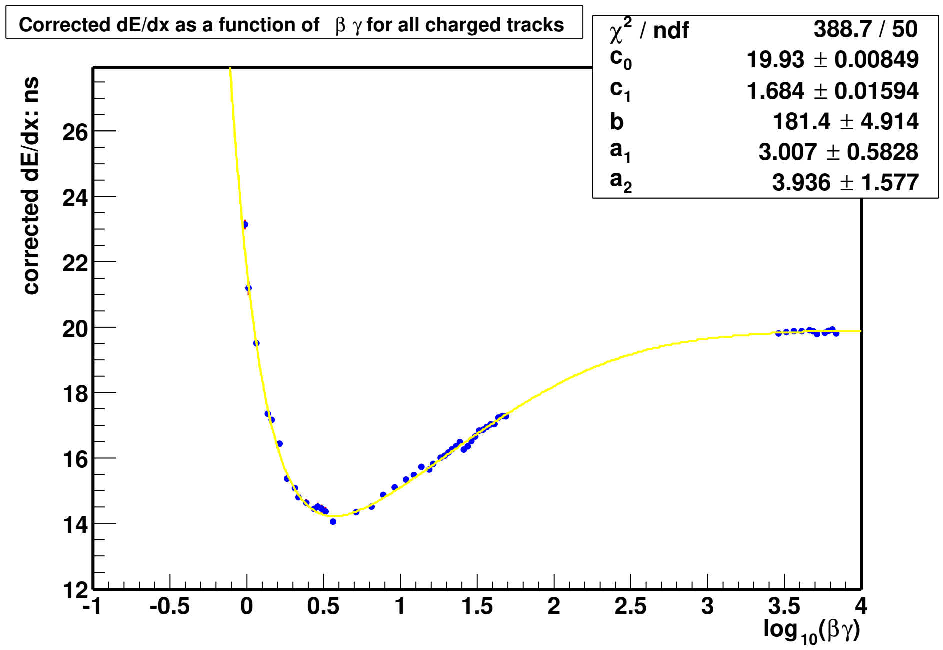

Figure 28: Universal curve for all charged tracks

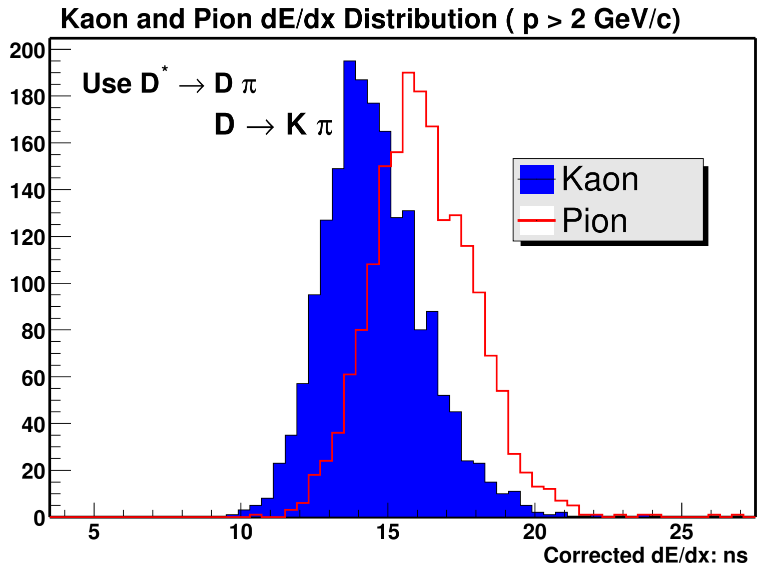

Figure 29: K, π dE/dx distribution, the number of events of two histograms are scaled to be equal.

5.3 $K - \pi$ Separation

With the samples of $D^* \to D\pi, D \to K\pi$, we can check the separation of kaons and pions in dE/dx. See Figure 29. The difference between the mean of the Gaussian fits is about 1.7 ns while the average of the two σs is 1.6 ns.[12] We confirm that current dE/dx calibration gives kaon and pion about 1 σ separation for momentum greater than 2 GeV$/c$, which is what is expected in the CDF Technical Design Report. [5] [9] The separation power stays about 1 σ for the momentum up to 10 GeV$/c$. It slowly decreases from 1 σ to 0.75 σ from the momentum 10 GeV$/c$ to 30 GeV$/c$.

[12]Note: The separation power given by computing the difference between two peaks is better than using the mean of the Gaussian fits.

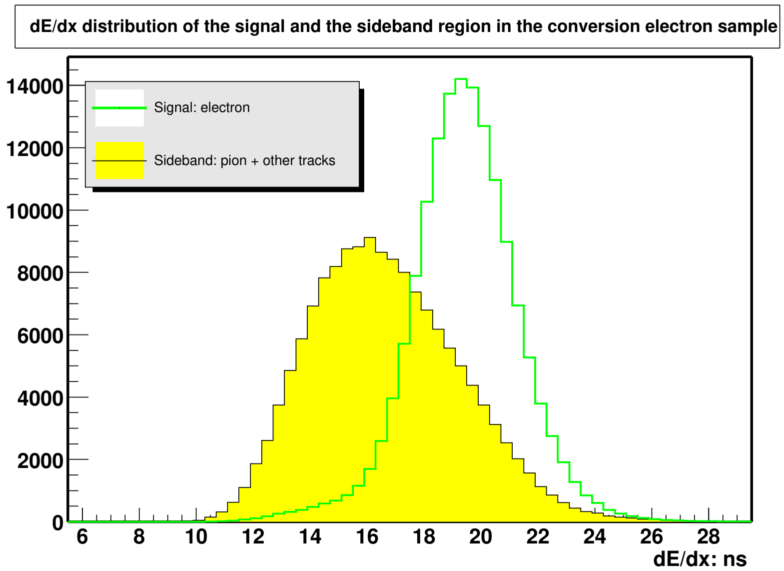

Figure 30: e, π dE/dx distribution, the number of events of two histograms are scaled to be equal.

5.4 $e - \pi$ Separation

With conversion samples, we can check the separation of electrons and pions in dE/dx by overlaying the dE/dx distributions from the signal region ($|\Delta \cot\theta| < 0.02$) and the side-band region ($\Delta \cot\theta > 0.06$). See Figure 30.

The difference between the mean of the Gaussian fits is about 2.7 ns while the average of the two σs is 2 ns.[13] The separation power stays above 2 σ for the momentum below 4 GeV/c, 1 σ for the momentum below 14 GeV/c. It decreases from 1 σ to 0.6 σ from the momentum 14 GeV/c to 30 GeV/c.

[13]Note: The separation power given by computing the difference between two peaks is better than using the mean of the Gaussian fits.

6 Conclusions

- With current calibrations, we have reached the expectation in the TDR and have $\sim 1\sigma$ separation for K and π above 2 GeV/c. We have also obtained two universal curves for the positive charged tracks and negative charged tracks.

- The electron identification using dE/dx meets the design specification in the CDF Run II Technical Design Report [9].

- When the luminosity of Tevatron goes up, we could also study the dependence on luminosity which has been seen in run I. [5] [8]

7 Acknowledgments

I would like to thank the whole Penn group, especially Joel Heinrich, who has helped me resolve many puzzles, also Dave Ambrose and Peter Wittich who have debugged and fixed ASDQ readout chain. They made the detector perfect. I shall also thank my adviser Nigel Lockyer who assigned me this project.

Thanks to Marjorie Shapiro and Barry Wicklund for providing their rich experience in run I and physics picture, to Hung-Chung Fang for studying the electron and hadron separation of different truncated mean and posing meaningful dE/dx questions, to Bill Orejudos who first wrote the interface of software for people to access dE/dx easily.

I also would like to thank Ayana Holloway for working on the ASDQ analog monitor and the flash ADC. Finally, thanks to Aseet Mukherjee, who helped me understand the physics of drift chamber through many interesting debates and discussions, and who also instrumented the pressure feedback circuit which significantly reduced the dE/dx dependence on the pressure.

References

[1] W. Blum, L. Rolandi. *Particle Detection with Drift Chambers*. Springer Verlag

[2] Particle Data Group. *The European Physical Journal C*

[3] Joel Heinrich. *COT Signal Simulation*. COT Workshop (ANL, May 1-2, 1998)

[4] M. Hauschild. *Progress in dE/dx Techniques Used for Particle Identification*. Nucl.Instrum.Meth. A379:436-441, 1996

[5] A. B. Wicklund, K. Byrum. *Calibrations and Applications of dE/dx from the CTC*. CDF note 2624

[6] H. Keutelian. *CTC dE/dx Applications Part I and II*

[7] Hung-Chung Fang. *Private communications*

[8] M. D. Peters. *Run 1B dE/dx Corrections*. CDF note 3807

[9] CDF Collaboration. *CDF II Technical Design Report*

[10] W. Riegler, K. Burkett, M. Franklin, C. Hall, A. Holloway, T. Jocobi, R. Madrak, M. Wessels. *COT Detector Physics Simulations*. CDF note 5050

[11] Bob Wagner (FNAL). *Private communications*